UC Berkeley
UC Berkeley Previously Published Works

Title

A Molecular Surface Functionalization Approach to Tuning Nanoparticle Electrocatalysts for Carbon Dioxide Reduction

Permalink

Journal

ISSN

Authors

Cao, Zhi
Kim, Dohyung
Hong, Dachao
et al.

Publication Date

DOI

A Molecular Surface Functionalization Approach to Tuning Nanoparticle Electrocatalysts for Carbon Dioxide Reduction

Zhi Cao,[†] Dohyung Kim,[‡] Dachao Hong,[†] Yi Yu,[†,#] Jun Xu,[†] Song Lin,[†,⊥] Xiaodong Wen,[∇,○] Eva M. Nichols,[†,⊥] Keunhong Jeong,[†] Jeffrey A. Reimer,[†] Peidong Yang,*[†,‡,#,◆] and Christopher J. Chang*[†,§,‖,⊥]

[†]Department of Chemistry, [‡]Department of Materials Science and Engineering, [§]Department of Molecular and Cell Biology, and [‖]Howard Hughes Medical Institute, University of California, Berkeley, California 94720, United States

[⊥]Chemical Sciences Division and [#]Materials Sciences Division, Lawrence Berkeley National Laboratory, Berkeley, California 94720, United States

[∇]Institute of Coal Chemistry, Chinese Academy of Sciences, Taiyuan, Shanxi 030001, China

[○]Synfuels China, Beijing 100195, China

[◆]Kavli Energy Nanosciences Institute, Berkeley, California 94720, United States

Ⓢ *Supporting Information*

ABSTRACT: Conversion of the greenhouse gas carbon dioxide (CO_2) to value-added products is an important challenge for sustainable energy research, and nanomaterials offer a broad class of heterogeneous catalysts for such transformations. Here we report a molecular surface functionalization approach to tuning gold nanoparticle (Au NP) electrocatalysts for reduction of CO_2 to CO. The *N*-heterocyclic (NHC) carbene-functionalized Au NP catalyst exhibits improved faradaic efficiency (FE = 83%) for

reduction of CO_2 to CO in water at neutral pH at an overpotential of 0.46 V with a 7.6-fold increase in current density compared to that of the parent Au NP (FE = 53%). Tafel plots of the NHC carbene-functionalized Au NP (72 mV/decade) vs parent Au NP (138 mV/decade) systems further show that the molecular ligand influences mechanistic pathways for CO_2 reduction. The results establish molecular surface functionalization as a complementary approach to size, shape, composition, and defect control for nanoparticle catalyst design.
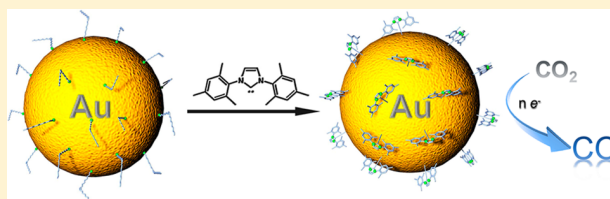
■ INTRODUCTION

Global climate change and energy demands have attracted interest in the sustainable, reductive transformation of carbon dioxide into value-added carbon products.[1,2] Electrochemical processes offer one method to meet this challenge, and much effort has been devoted to searching for catalysts with high efficiency and selectivity for the electrochemical reduction of CO_2.[3,4] Among existing classes of catalysts, heterogeneous inorganic materials are attractive as they offer high conductivity and aqueous compatibility with the ability to provide good selectivity.[5−10] In particular, recent advances in the controlled synthesis of metal nanoparticles (NPs) provide opportunities to systematically explore catalytic properties as a function of surface area and morphology. Indeed, a number of metal NPs including Au, Cu, and Ag have been investigated as heterogeneous catalysts for the electrochemical reduction of CO_2 to carbon monoxide, methane, and formate.[11−16] Efforts to tailor the catalytic performance of metal NPs have been largely limited to tuning particle size,[11−13] shape,[14] composition,[15] and defect sites.[7,17,18] Nafion coating has been demonstrated to promote the CO_2 activity of Au nanoparticle electrocatalysts.[19] However, lack of molecular tunability of the nafion binder hinders its further application. As such, systematic

optimization of the electronic structure of metal NP electro-catalysts at a molecular level remains a challenge. We now report molecular surface functionalization as a complementary design concept to tuning metal NP catalysts, as illustrated using NHC carbene-functionalized Au NPs that show improved properties over their parent Au NP counterparts for electro-catalytic CO_2 reduction.

We recently initiated a broad-based program on hybrid molecular materials[20,21] and materials biology[22−24] platforms for CO_2 reduction and related energy catalysis. On the molecular-materials side, we and others recently reported catalysts for selective and active CO_2 to CO reduction in water through incorporating tunable molecular units within extended covalent−organic frameworks (COFs)[20] and their metal−organic framework (MOF) congeners.[8,21,25,26] One key advantage of such hybrid materials is that their performance may be optimized using fundamental molecular chemistry principles. We envisioned that a similar molecular-materials approach may also be used to design new classes of metal NP catalysts. In particular, we were inspired by recent advances in

organometallic Au chemistry, where careful design and modification of ligand structures has led to novel reactivity of small molecule Au-complexes.[27] Indeed, Au catalysis has been broadly applied to homogeneous catalysis of organic reactions including C−H activation, cross-coupling, and enyne cyclization.[28−33] In particular, we recognized that NHC carbenes are a versatile family of ligands for Au catalysis[34] and noted parallel work where these ligands can also be used to modify metallic gold with good stability under acidic, thermal conditions.[35] These precedents encouraged us to pursue molecular surface functionalization as a design approach to tune the reactivity of Au NPs in electrochemical CO_2 reduction, where the molecular-material hybrids can be thought of as heterogeneous analogs to homogeneous organometallic complexes.

■ RESULTS AND DISCUSSION

The oleylamine-capped Au NPs (Au−Oa NP) were prepared in a manner based on our previously reported method.[15] The carbene-functionalized Au NPs were synthesized according to modified literature precedent.[36−39] A general scheme for the synthesis of NHC carbene-functionalized Au NPs is illustrated in Figure 1a. Upon addition of excess 1,3-bis(2,4,6-
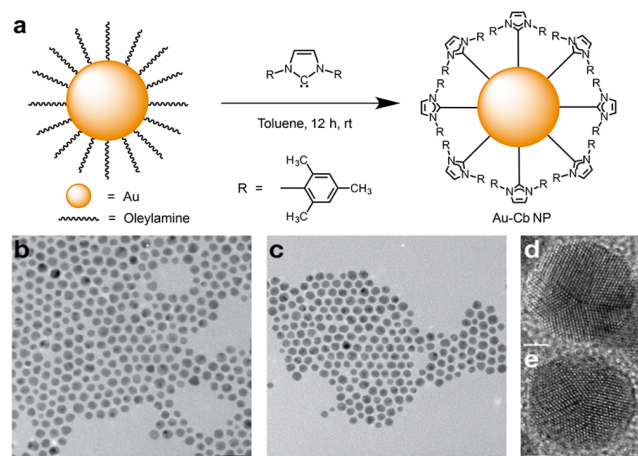

Figure 1. (a) Scheme of Cb ligand exchange reaction on Au NPs. TEM image of (b) Au−Oa NP and (c) Au−Cb NP, scale bar, 20 nm. HRTEM image of (d) Au−Oa NP and (e) Au−Cb NP with 5-fold twin structures, scale bar, 2 nm.

trimethylphenyl)imidazol-2-ylidene (Cb) in anhydrous toluene and washing with toluene to remove uncoordinated Cb ligand, the resulting dark purple precipitate, here designated as Au−Cb NP, was collected by centrifugation, characterized, and subsequently used in electrocatalytic studies.

Transmission electron microscopy (TEM) studies reveal that Au−Cb NP resulting from ligand exchange possess morphology nearly identical to that of the Au−Oa NP precursor (Figure 1b,c). The size distribution of the two types of particles is comparable, with an average particle size of approximately 7 nm (Figure S1). The crystallinity of the particles is also similar, as evident by X-ray diffraction studies (Figure S2). High-resolution transmission electron microscopy (HRTEM) was used to characterize the morphology and surface structure of both types of NPs at an atomic level as these features are believed to be key to catalyst performance in many electrochemical processes.[6,11,14] The parent oleylamine-capped Au NPs mainly have 5-fold twin structures with decahedral and icosahedral morphologies (Figures 1d and S3), typical for face-

centered cubic nanocrystals.[40] HRTEM studies on Au−Cb NP reveal that nanoparticles after ligand exchange still show both morphologies (Figures 1e and S3).

To confirm successful Cb ligand exchange, both Au−Oa NP and Au−Cb NP were analyzed by Fourier transform infrared spectroscopy (FT-IR) (Figure 2a). The FT-IR spectra of Au−
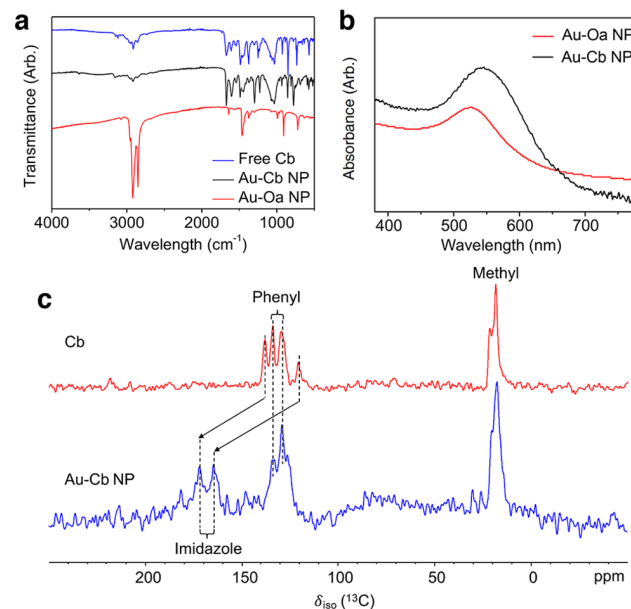

Figure 2. (a) FT-IR spectra of free NHC carbene (Cb), Au−Cb NP, and Au−Oa NP. (b) UV−vis spectra of Au−Oa NP recorded in hexanes and Au−Cb NP in DMSO. (c) Solid-state ^{13}C NMR spectra of free carbene and Au−Cb NP.

Oa NP show features originating from the surface-capping oleylamine ligands, mainly hydrocarbon chain vibrational modes (ν_{as}(C−H) ≈ 2922 cm^{-1}, ν_s(C−H) ≈ 2853 cm^{-1}, δ(−C=C) ≈ 1643 cm^{-1}, δ(CH$_3$) ≈ 1467 cm^{-1}, and δ(C−C) ≈ 722 cm^{-1} where ν_{as}, ν_s, and δ stand for asymmetric stretching, symmetric stretching, and bending modes respectively).[41] In contrast, Au−Cb NP exhibits new spectral features bearing extensive similarity to that of the free Cb ligand and an absence of hydrocarbon modes, suggesting successful Cb ligand exchange.

The UV−vis spectrum of Au−Oa NP in hexanes displays a characteristic maximum absorption at ca. 525 nm (Figure 2b), a result of surface plasmonic resonance. Following ligand substitution, the Au−Cb NP was no longer dispersible in nonpolar organic solvents. Nevertheless, the surface plasmonic resonance peak for Au−Cb NP in DMSO is observed at ca. 543 nm (Figure 2b), indicating that the resultant NPs are well-stabilized in this matrix. The slight red-shift of the surface plasmonic resonance peak of Au−Cb NP is attributed to the larger refractive index of DMSO compared to hexanes.[42]

Coordination of the Cb ligands to the Au NP surface was further verified using nuclear magnetic resonance (NMR) spectroscopy. Solid-state ^{13}C NMR spectra of free Cb and Au−Cb NP (Figure 2c) demonstrate coordination of the Cb ligands to the Au nanoparticles: The two ^{13}C peaks of free Cb at 120.4 and 133.9 ppm, which are characteristic of imidazole, shift to 164.7 and 172.0 ppm as a result of donation of electron density from the molecular ligands to gold.

With materials characterization data in hand, we compared the electrochemical reduction of CO_2 to CO catalzyed by Au–Cb NP and bare Au nanoparticles (as a comparison for the activity of the Au–Cb NP) using a custom-made electrochemical cell with 0.1 M $KHCO_3$ (pH 6.8) as electrolyte. For the bare Au NP, to prevent nanoparticle sintering, Au–Oa NP was first loaded onto carbon black by sonication to make an Au–Oa NP/C composite and followed by thermal annealing to remove the oleylamine capping ligand,[11] affording an Au NP/C composite. This composite was then deposited onto a carbon electrode to prepare the Au NP/C working electrode. The morphology of Au–Oa NP/C composite (before thermal treatment) and Au NP/C composite (after thermal treatment) was monitored by TEM (Figure S4). After thermal treatment, there is no noticeable change for Au NP/C composite. The FT-IR spectrum of thermally treated Au-Oa NP/C revealed that the IR spectral features of oleylamine disappeared (Figure S5). For the Au–Cb NP working electrode, which is prepared without thermal annealing, the Au–Cb NP was redispersed in chloroform and directly drop-cast onto a carbon paper electrode. The electrochemically active surface area for both Au NP/C and Au–Cb NP electrode was evaluated by using Pb underpotential deposition (upd).[17,43,44] All electrodes displayed two significant peaks in the Pb-upd voltammograms (arising from Au (111) and (110) facets), as shown in Figure 3. According to the Pb-upd voltammogram results, Au NP/C and Au–Cb NP electrodes have a Au surface area of 0.674 and 0.342 cm^2, respectively.
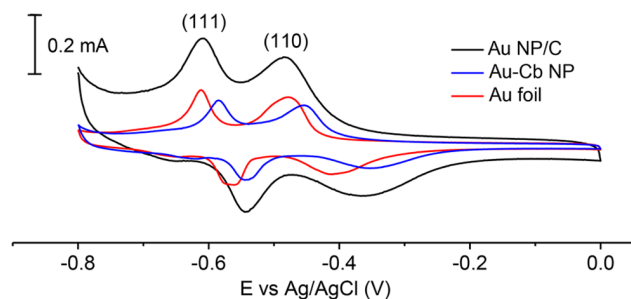

Figure 3. Pb-upd profiles of the Au NP/C, Au–Cb NP, and polycrystalline Au foil (0.7 cm × 0.7 cm) electrodes. The peak area of both Au NP/C and Au–Cb NP was referenced to the geometric area of the Au foil. Scan rate: 50 mV/s.

The CO_2 reduction activity of Au nanoparticle catalysts in CO_2-saturated $KHCO_3$ was evaluated by linear sweep voltammetry (LSV) studies (Figure 4a). All potentials reported herein are referenced to the reversible hydrogen electrode (RHE) except for Pb-upd results. The Au–Cb NP catalyst exhibits larger total current densities and positively shifted onset potentials relative to Au NP/C. The −0.26 V onset potential corresponds to a 150 mV overpotential, given the equilibrium potential of −0.11 V (vs RHE) for CO_2/CO couple at pH 6.8. The onset potential at −0.26 V reflects a prominent catalytic effect of Au–Cb NP on the reduction of CO_2 in neutral aqueous media. To exclude possibility that a species other than Au–Cb NP is responsible for the CO_2 reduction activity, control LSV scans were performed on the free carbene and a molecular Au–Cb complex (chloro[1,3-bis(2,4,6-trimethylphenyl)imidazol-2-ylidene]gold(I)), as shown in Figure 4a. Under CO_2-saturated conditions, both
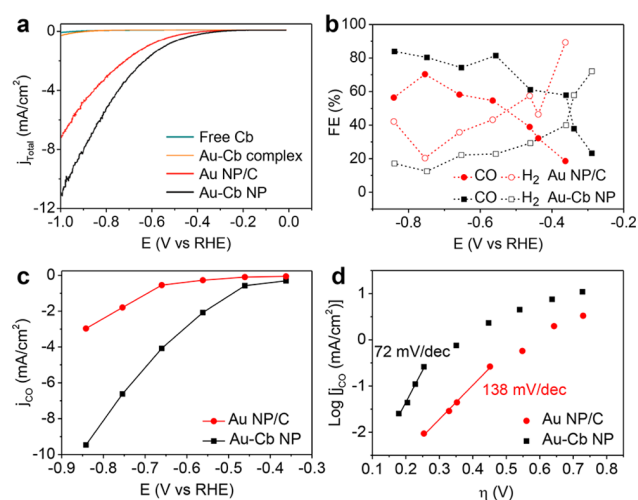

Figure 4. (a) LSV scans of Au–Cb NP, Au NP/C, free carbene and molecular Au–Cb complex under CO_2-saturated 0.1 M $KHCO_3$ at pH 6.8. (b) Faradaic efficiencies of products formed from Au–Cb NP and Au NP/C. (c) Specific CO current density (based on electrochemically active surface area) plots for Au–Cb NP and Au NP/C. (d) Tafel plots of Au–Cb NP and Au NP/C.

control materials showed a minimal current response, revealing that catalytic activity is unique to the Au–Cb NP.

Controlled potential electrolyses were performed in CO_2-saturated $KHCO_3$ buffer under applied potentials between −0.27 and −0.87 V to confirm CO_2 reduction. Gaseous products were analyzed by gas chromatography (GC), and liquid products were characterized by proton nuclear magnetic resonance (^{1}H NMR) spectroscopy. Two major gas products, CO and H_2, were generated with both Au–Cb NP and Au NP/C as the catalyst. A trace amount of formate (<1%) was also detected with Au–Cb NP (Figure S6).

The dependence of faradaic efficiencies (FEs) for CO and H_2 on the applied potentials of both Au–Cb NP and Au NP/C is shown in Figure 4b. Across all applied potentials examined, the Au–Cb NP catalyst shows higher FEs for CO and lower FEs for H_2 compared to that of the Au NP/C catalyst. At −0.57 V (η = 460 mV), the Au–Cb NP catalyst displays optimal performance for CO production (FE = 83%). More positive potentials promoted off-target water reduction to hydrogen, whereas more negative potentials require more electrical energy input but show no noticeable difference in CO FEs. It is also noteworthy that the H_2 production can be suppressed to only 13% at −0.75 V. The specific current density (j_{CO}, is normalized to electrochemically active Au surface area) as a function of applied potential for both Au NP/C and Au–Cb NP was extracted from data of the controlled potential electrolyses (Figure 4c), showing a higher value for Au–Cb NP.

To evaluate whether catalytic activity can be tuned by the steric demands of the surface-bound ligand, two additional NHC carbenes were also used to functionalize Au nanoparticles: 1,3-bis(2,6-diisopropylphenyl)-1,3-dihydro-2*H*-imidazol-2-ylidene (Cb2) and 1,3-di*tert*-butylimidazol-2-ylidene (Cb3). These carbene-functionalized Au nanoparticles were also evaluated as catalysts for electrochemical reduction of CO_2 to CO under the same conditions as those of Au–Cb NP and Au NP/C. The faradaic efficiencies of produced CO of all four catalysts are shown in Figure S7. Across the applied potential window (−0.37 to −0.87 V), carbene-functionalized Au nanoparticles outperform the Au NP/C in terms of CO

selectivity, revealing that NHC carbene surface functionalization promotes CO_2 reduction activity. Among the three carbene-functionalized Au NP catalysts, Au—Cb NP exhibits the highest CO selectivity, followed by Au—Cb2 NP, and then Au—Cb3. Because the donor strength of these three carbenes is similar, differences in activity can instead be attributed to sterics. A common descriptor for the steric bulk of NHC carbenes, analogous to the Tolman cone angle for phosphines, is the percent buried volume, or $\%V_{bur}$. The $\%V_{bur}$ for Cb, Cb2, and Cb3 is 31.6, 33.6, and 35.5%, respectively.[45] Thus, our results indicate that increasing steric bulk of the carbene appears to lower the faradaic efficiency for CO.[45]

The stability of Au—Cb NP under electrochemical conditions was evaluated by FT-IR, Pb-upd, and ^{13}C solid-state NMR. Au—Cb NP catalyst from the same electrode exhibits nearly identical FT-IR signals before and after electrolysis, reflecting its electrochemical stability (Figure 5a). Similarly, the electro-
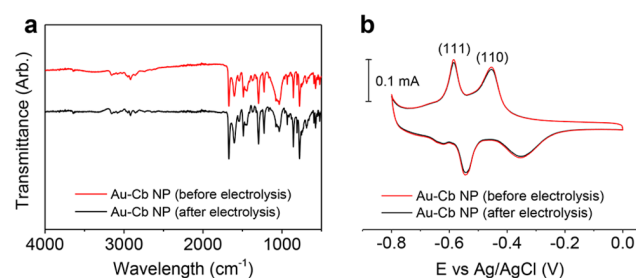

Figure 5. (a) FT-IR spectra of Au—Cb NP before and after electrolysis; (b) Pb-upd profiles of the Au—Cb NP before and after electrolysis. Scan rate: 50 mV/s.

chemically accessible Au surface area for the same Au—Cb NP working electrode before and after electrolysis was nearly identical as evidenced by the equal peak areas of Au (111) and (110) in a lead underpotential deposition experiment (Figure 5b). Finally, a comparison of ^{13}C solid-state NMR spectra of the Au—Cb NP electrode before and after electrolysis shows that all assigned C peaks of surface functionalized carbene are consistent (Figure S8).

The kinetics of CO_2 reduction at Au NP/C and Au—Cb NP were examined using Tafel analysis (Figure 4d). The results unambiguously demonstrate that Cb functionalization at the Au nanoparticle surface influences the mechanistic pathways for CO_2 reduction. A Tafel plot of the logarithm of current density $[\log(j_{CO})]$ versus overpotential (η) gives a slope of 138 mV/decade for Au NP/C, which is comparable to the 118 mV/decade expected for rate-limiting single-electron transfer from the adsorbed CO_2 to generate the surface-adsorbed $CO_2^{\bullet-}$. In contrast, the Tafel slope for Au—Cb NP is only 72 mV/decade, indicating that Au—Cb NP are very likely to undergo a pre-equilibrating one-electron transfer followed by a rate-limiting chemical step. It has been proposed that the cation of imidazolium-based ionic liquids may be reduced to the neutral NHC carbene under electrochemical conditions, and this free carbene may be responsible for enhancing CO_2 reduction activity.[46,47] However, because we observe strong binding of the carbene to the gold surface, we do not expect imidazolium/free carbene to play a large role and speculate that carbene coordination may influence the gold surface through a combination of both electronic and geometric effects. Strong σ-donation from the carbenes makes the gold NP surface highly electron rich, which may explain the observed change in

mechanism for Au—Cb NP in which a fast electron transfer to CO_2 occurs prior to the rate-determining step. Similar electronic effects have been invoked to explain enhancements in activity of platinum nanowires in the partial hydrogenation of nitroaromatics.[48] From a geometric perspective, the strong carbene—gold bond can destabilize gold—gold bonding with neighboring atoms[49] (Figure S9). This destabilization may lead to restructuring of the Au NP surface, thereby increasing the number of defect sites with better kinetics for the CO_2 reduction reaction. Related examples of chemisorbed molecules inducing significant surface restructuring have been documented; for instance, C on Ni(100) causes Ni atom displacement[50,51] and S on Fe(100) leads to Fe—S cluster formation.[52]

■ CONCLUSIONS

We have described a molecular surface functionalization approach to tuning metal NP catalysts, illustrated by improving the electrocatalytic reduction of CO_2 to CO in water by Au nanoparticles through coordination to molecular NHC carbene ligands. We anticipate that this organometallic strategy, where heterogeneous, hybrid molecular-material analogs to homogeneous coordination complexes can be designed, synthesized, and characterized, will be applicable for a wide range of catalytic applications. We are particularly interested in expanding this chemical concept to reactions that require sustainable energy input and aqueous compatibility.

■ EXPERIMENTAL DETAILS

Chemicals. Oleylamine, 1-octadecene, oleic acid, 1,2-hexadecanediol, 1,3-bis(2,4,6-trimethylphenyl)imidazol-2-ylidene, 1,3-bis(2,6-diisopropylphenyl)-1,3-dihydro-2H-imidazol-2-ylidene, 1,3-di-*tert*-butyli-midazol-2-ylidene, potassium bicarbonate (≥99.99% trace metals basis, 99.7−100.5% dry basis), and silver wire (99.9% trace metal basis, 0.5 mm diameter) were purchased from Sigma-Aldrich. Gold acetate, platinum wire (0.5 mm dia, Premion, 99.997%), and Toray Carbon Paper (TGP-H-60) were from Alfa Aesar. Deionized water was from a Millipore Autopure system. All reagents were of analytical grade and used without further purification. Carbon dioxide (5.0 UHP) and Argon (5.0 UHP) gas were purchased from Praxair.

Syntheses and Physical Characterizations. *Synthesis of Au—Oa NP.* Au nanoparticles were synthesized via the reduction of Au precursor in organic solvent.[15] 1-Octadecene (20 mL) was heated to 130 °C for 30 min under nitrogen atmosphere. Then, 2 mmol of oleic acid, 2 mmol of oleylamine, 0.6 mmol of gold acetate, and 4 mmol of 1,2-hexadecanediol were subsequently added after cooling it down to room temperature. Under N_2 atmosphere, the mixture was heated to 200 °C and kept at the same temperature for 2 h while stirring. The reaction was stopped by cooling it down to room temperature. The product was precipitated by ethanol and collected by centrifugation (8000 rpm, 5 min). The final product was dispersed in toluene for further use and exhibited significant stability in ambient atmosphere.

Synthesis of Au—Cb NP. Under an inert atmosphere, 3 mL (2 mg/mL in toluene) of Au—Oa NP was dissolved in 5 mL of toluene, and 200 times excess of Cb ligand was added in a solid portion.[35] The particles were left to crash out for 12 h, with no stirring. Reactions performed under standard Schlenk technique gave the best quality Au—Cb NP. The particles were then centrifuged (5000 rpm, 5 min) and washed with 5 mL of toluene. This process was repeated three times, and obtained Au—Cb NP was then dried under vacuum before use.

Physical Characterization. Catalyst morphology was characterized by TEM (Hitachi H7650). HRTEM images were recorded using a FEI Tecnai G20 with an accelerating voltage of 200 kV. XRD patterns of the catalysts were collected on a Bruker D8-Advanced diffractometer with Cu Kα radiation (λ = 1.5406 Å). The solution of nanoparticles

were characterized by UV−vis spectroscopy (Vernier). IR spectra were recorded with a Burker ALPHA FT-IR spectrometer fitted with a diamond ATR module. Solid-state ^{13}C cross-polarization (CP) magic-angle spinning (MAS) NMR experiments were performed on a Tecmag Discovery spectrometer at 7.04 T using a Doty 4 mm triple-resonance probe. Parameters of SSNMR experiments including CP condition, pulse delay, and contact time were optimized prior to data acquisition. The spinning rate is 10 kHz. ^{13}C chemical shift was referenced to the methylene signal of adamantane, which is 38.48 ppm relative to TMS.

Electrochemically Accessible Surface Area Measurement. The electrochemical surface area of working electrodes was determined by measuring the charge associated with the stripping of an under-potential deposited (upd) Pb monolayer.[17] The electrode was immersed in a 0.1 M KOH solution containing 1 mM Pb(OAc)$_2$ continuously purged with Ar in a two-compartment electrochemical cell. Pt gauze was used as the reference electrode, and Ag/AgCl (3 M KCl) was used as the reference electrode. Cyclic voltammagrams from 0 to −0.8 V with a scan rate of 50 mV/s were acquired repeatedly until traces converged. The anodic stripping wave responsible for Au (110) was integrated. The surface area of the Au NP and Au−Cb NP electrodes was calculated by normalizing to the integral of the same stripping wave of Au foil with a known area.

CO$_2$ Reduction Measurements. *Preparation of the Working Electrode.* For Au NP/C catalyst, Au−Oa NP was first loaded onto carbon black (Super P) by sonication to make Au−Oa NP/C composite,[11] followed by thermal annealing overnight in air at 165 °C to remove the oleylamine capping ligand, affording Au NP/C composite. This Au NP/C composite was then deposited on a carbon paper to prepare the Au NP/C working electrode, which was used for subsequent electrochemical measurements. For Au−Cb NP catalyst, Au−Cb NP was redispersed in chloroform and directly drop-cast onto a carbon paper electrode. The prepared working electrodes were dried under vacuum at room temperature before use.

Electrochemical Measurements. All the experiments were carried out in our customized electrochemical setup which has two compartments. The two compartments separate working and counter electrodes with an anion-exchange membrane (Selemion AMV). Each compartment holds 20 mL of electrolyte, and the working compartment is sealed in order to allow measurements of gaseous products. Platinum wire was used as a counter electrode and Ag/AgCl (in 1 M KCl) as a reference electrode. All potentials in this study were measured against the Ag/AgCl reference electrode and converted to the RHE reference scale by E (vs RHE) = E (vs Ag/AgCl) + 0.236 V + 0.0591 × pH. The electrolyte was prepared according to literature procedure.[15]

Electrolyte (0.1 M KHCO$_3$) was saturated with CO$_2$ (pH 6.8) at a flow rate of 30 sccm for at least 20 min under stirring conditions. Linear sweep voltammetry was conducted initially at a scan rate of 50 mV/s and multiple working electrodes prepared for each sample showed similar performance in terms of current output. During chronoamperometry, effluent gas from the cell went through the sampling loop of a gas chromatograph (SRI) to analyze the concentration of gas products. The gas chromatograph was equipped with a molecular sieve 13X (1/8" × 6') and hayesep D (1/8" × 6') column with Ar flowing as a carrier gas. The separated gas products were analyzed by a thermal conductivity detector (for H$_2$) and a flame ionization detector (for CO). Quantification of the products was performed with the conversion factor derived from the standard calibration gases. Liquid products were analyzed afterward by qNMR (Bruker AV-500) using dimethyl sulfoxide as an internal standard. Solvent presaturation technique was implemented to suppress the water peak. Faradaic efficiencies were calculated from the amount of charge passed to produce each product divided by the total charge passed at a specific time or during the overall run.

ASSOCIATED CONTENT

Ⓢ Supporting Information

The Supporting Information is available free of charge on the ACS Publications website at DOI: 10.1021/jacs.6b02878.

Experimental details and data (PDF)

AUTHOR INFORMATION

Corresponding Authors
*E-mail: p_yang@berkeley.edu.
*E-mail: chrischang@berkeley.edu.

Author Contributions
Z.C. and D.K. contributed equally to this work.

Notes
The authors declare no competing financial interest.

REFERENCES

(1) Lewis, N. S.; Nocera, D. G. *Proc. Natl. Acad. Sci. U. S. A.* **2006**, *103*, 15729.
(2) Gray, H. B. *Nat. Chem.* **2009**, *1*, 7.
(3) Costentin, C.; Robert, M.; Savéant, J.-M. *Chem. Soc. Rev.* **2013**, *42*, 2423.
(4) Kim, D.; Sakimoto, K. K.; Hong, D.; Yang, P. *Angew. Chem., Int. Ed.* **2015**, *54*, 3259.
(5) Li, C. W.; Ciston, J.; Kanan, M. W. *Nature* **2014**, *508*, 504.
(6) Chen, Y.; Li, C. W.; Kanan, M. W. *J. Am. Chem. Soc.* **2012**, *134*, 19969.
(7) Hall, A. S.; Yoon, Y.; Wuttig, A.; Surendranath, Y. *J. Am. Chem. Soc.* **2015**, *137*, 14834.
(8) Hod, I.; Sampson, M. D.; Deria, P.; Kubiak, C. P.; Farha, O. K.; Hupp, J. T. *ACS Catal.* **2015**, *5*, 6302.
(9) Zhang, S.; Kang, P.; Meyer, T. J. *J. Am. Chem. Soc.* **2014**, *136*, 1734.
(10) Zhang, S.; Kang, P.; Ubnoske, S.; Brennaman, M. K.; Song, N.; House, R. L.; Glass, J. T.; Meyer, T. J. *J. Am. Chem. Soc.* **2014**, *136*, 7845.
(11) Zhu, W.; Michalsky, R.; Metin, O. n.; Lv, H.; Guo, S.; Wright, C. J.; Sun, X.; Peterson, A. A.; Sun, S. *J. Am. Chem. Soc.* **2013**, *135*, 16833.
(12) Reske, R.; Mistry, H.; Behafarid, F.; Roldan Cuenya, B.; Strasser, P. *J. Am. Chem. Soc.* **2014**, *136*, 6978.
(13) Mistry, H.; Reske, R.; Zeng, Z.; Zhao, Z.-J.; Greeley, J.; Strasser, P.; Cuenya, B. R. *J. Am. Chem. Soc.* **2014**, *136*, 16473.
(14) Zhu, W.; Zhang, Y.-J.; Zhang, H.; Lv, H.; Li, Q.; Michalsky, R.; Peterson, A. A.; Sun, S. *J. Am. Chem. Soc.* **2014**, *136*, 16132.
(15) Kim, D.; Resasco, J.; Yu, Y.; Asiri, A. M.; Yang, P. *Nat. Commun.* **2014**, *5*, 4948.
(16) Gao, D.; Zhou, H.; Wang, J.; Miao, S.; Yang, F.; Wang, G.; Wang, J.; Bao, X. *J. Am. Chem. Soc.* **2015**, *137*, 4288.

(17) Feng, X.; Jiang, K.; Fan, S.; Kanan, M. W. *J. Am. Chem. Soc.* **2015**, *137*, 4606.

(18) Wuttig, A.; Surendranath, Y. *ACS Catal.* **2015**, *5*, 4479.

(19) Andrews, E.; Katla, S.; Kumar, C.; Patterson, M.; Sprunger, P.; Flake, J. *J. Electrochem. Soc.* **2015**, *162*, F1373.

(20) Lin, S.; Diercks, C. S.; Zhang, Y.-B.; Kornienko, N.; Nichols, E. M.; Zhao, Y.; Paris, A. R.; Kim, D.; Yang, P.; Yaghi, O. M.; Chang, C. J. *Science* **2015**, *349*, 1208.

(21) Kornienko, N.; Zhao, Y.; Kley, C. S.; Zhu, C.; Kim, D.; Lin, S.; Chang, C. J.; Yaghi, O. M.; Yang, P. *J. Am. Chem. Soc.* **2015**, *137*, 14129.

(22) Liu, C.; Gallagher, J. J.; Sakimoto, K. K.; Nichols, E. M.; Chang, C. J.; Chang, M. C. Y.; Yang, P. *Nano Lett.* **2015**, *15*, 3634.

(23) Nichols, E. M.; Gallagher, J. J.; Liu, C.; Su, Y.; Resasco, J.; Yu, Y.; Sun, Y.; Yang, P.; Chang, M. C. Y.; Chang, C. J. *Proc. Natl. Acad. Sci. U. S. A.* **2015**, *112*, 11461.

(24) Sakimoto, K. K.; Wong, A. B.; Yang, P. *Science* **2016**, *351*, 74.

(25) Wang, C.; Xie, Z.; deKrafft, K. E.; Lin, W. *J. Am. Chem. Soc.* **2011**, *133*, 13445.

(26) Wang, C.; Liu, D.; Lin, W. *J. Am. Chem. Soc.* **2013**, *135*, 13222.

(27) Gorin, D. J.; Sherry, B. D.; Toste, F. D. *Chem. Rev.* **2008**, *108*, 3351.

(28) Hashmi, A. S. K. *Chem. Rev.* **2007**, *107*, 3180.

(29) Li, Z.; Brouwer, C.; He, C. *Chem. Rev.* **2008**, *108*, 3239.

(30) Dorel, R.; Echavarren, A. M. *Chem. Rev.* **2015**, *115*, 9028.

(31) Wang, Y.-M.; Lackner, A. D.; Toste, F. D. *Acc. Chem. Res.* **2014**, *47*, 889.

(32) Zhang, L. *Acc. Chem. Res.* **2014**, *47*, 877.

(33) Marion, N.; Nolan, S. P. *Chem. Soc. Rev.* **2008**, *37*, 1776.

(34) Hashmi, A. S. K. *Acc. Chem. Res.* **2014**, *47*, 864.

(35) Crudden, C. M.; Horton, J. H.; Ebralidze, I. I.; Zenkina, O. V.; McLean, A. B.; Drevniok, B.; She, Z.; Kraatz, H.-B.; Mosey, N. J.; Seki, T.; et al. *Nat. Chem.* **2014**, *6*, 409.

(36) Hurst, E. C.; Wilson, K.; Fairlamb, I. J. S.; Chechik, V. *New J. Chem.* **2009**, *33*, 1837.

(37) Ling, X.; Schaeffer, N.; Roland, S.; Pileni, M.-P. *Langmuir* **2013**, *29*, 12647.

(38) Vignolle, J.; Tilley, T. D. *Chem. Commun.* **2009**, 7230.

(39) Serpell, C. J.; Cookson, J.; Thompson, A. L.; Brown, C. M.; Beer, P. D. *Dalton Trans.* **2013**, *42*, 1385.

(40) Hofmeister, H. In *Encyclopedia of Nanoscience and Nanotechnology*; Schwarz, J. A., Contescu, C. I., Putyera, K., Eds.; Marcel Dekker: New York, 2004; Vol. 3, p 431.

(41) Mourdikoudis, S.; Liz-Marzán, L. M. *Chem. Mater.* **2013**, *25*, 1465.

(42) Mahmoud, M. A.; Chamanzar, M.; Adibi, A.; El-Sayed, M. A. *J. Am. Chem. Soc.* **2012**, *134*, 6434.

(43) Hamelin, A. *J. Electroanal. Chem. Interfacial Electrochem.* **1984**, *165*, 167.

(44) Hamelin, A.; Lipkowski, J. *J. Electroanal. Chem. Interfacial Electrochem.* **1984**, *171*, 317.

(45) Poater, A.; Cosenza, B.; Correa, A.; Giudice, S.; Ragone, F.; Scarano, V.; Cavallo, L. *Eur. J. Inorg. Chem.* **2009**, *2009*, 1759.

(46) Rosen, B. A.; Haan, J. L.; Mukherjee, P.; Braunschweig, B.; Zhu, W.; Salehi-Khojin, A.; Dlott, D. D.; Masel, R. I. *J. Phys. Chem. C* **2012**, *116*, 15307.

(47) Feroci, M.; Chiarotto, I.; Forte, G.; Vecchio Cipriori, S.; Inesi, A. *ChemElectroChem* **2014**, *1*, 1407.

(48) Chen, G.; Xu, C.; Huang, X.; Ye, J.; Gu, L.; Li, G.; Tang, Z.; Wu, B.; Yang, H.; Zhao, Z. *Nat. Mater.* **2016**, *15*, 564.

(49) Rodríguez-Castillo, M.; Laurencin, D.; Tielens, F.; Van der Lee, A.; Clément, S.; Guari, Y.; Richeter, S. *Dalton Trans.* **2014**, *43*, 5978.

(50) Gauthier, Y.; Baudoing-Savois, R.; Heinz, K.; Landskron, H. *Surf. Sci.* **1991**, *251-252*, 493.

(51) Onuferko, J. H.; Woodruff, D. P.; Holland, B. W. *Surf. Sci.* **1979**, *87*, 357.

(52) Shih, H. D.; Jona, F.; Jepsen, D. W.; Marcus, P. M. *Phys. Rev. Lett.* **1981**, *46*, 731.